TACAN is a novel regulator of PKD2

Xiong Liu[1#], Rui Zhang[2#], Mohammad Fatehi[3#], Yifang Wang[2], Wentong Long[3], Rui Tian[2], Xiaoling Deng[2], Ziyi Weng[2], Qinyi Xu[1], Peter E Light[3], Jingfeng Tang[2], Xing-Zhen Chen[1*]

[1]Membrane Protein Disease Research Group, Department of Physiology, Faculty of Medicine and Dentistry, University of Alberta, T6G 2H7, Edmonton, AB, Canada

[2]National "111" Center for Cellular Regulation and Molecular Pharmaceutics, Hubei University of Technology, Wuhan, Hubei 430068, China

[3]Department of Pharmacology, Faculty of Medicine and Dentistry, University of Alberta, T6G 2H7, Edmonton, Alberta, Canada.

[*]Correspondence: Xing-Zhen Chen (xzchen@ualberta.ca)

[#]These authors contributed equally.

Abstract

Autosomal dominant polycystic kidney disease (ADPKD) is caused by mutations in membrane receptor PKD1 or cation channel PKD2. TACAN (also named TMEM120A), recently reported as an ion channel in neuron cells for mechano and pain sensing, is also distributed in diverse non-neuronal tissues such as kidney, heart and intestine, suggesting its involvement in other functions. In this study, we found that TACAN is in complex with PKD2 in native renal cell lines. Using the two-electrode voltage clamp in *Xenopus* oocytes we found that TACAN inhibited the channel activity of PKD2 gain-of-function mutant F604P. The first and last transmembrane domains of TACAN were found to interact with the PKD2 C- and N-terminal portions, respectively. We showed that the TACAN N-terminus acted as a blocking peptide and that TACAN inhibits the PKD2 function through the PKD2/TACAN binding. By patch clamping in mammalian cells, we found that TACAN inhibits both the single channel conductance and open probability of PKD2 and mutant F604P. Further, PKD2 co-expressed with TACAN, but not PKD2 alone, exhibited pressure sensitivity. In summary, this study revealed that TACAN acts as a PKD2 inhibitor and mediates mechano sensitivity of the PKD2/TACAN channel complex.

Keywords: ADPKD, TMEM120A, electrophysiology, *Xenopus* oocyte, mammalian cell, zebrafish, CRISPR/Cas9

Introduction

Autosomal dominant polycystic kidney disease (ADPKD), characterized by accumulation of multiple cysts in both kidneys, is one of the most common human genetic diseases (Harris and Torres, 2009). Extrarenal pathologies associated with ADPKD may include hepatic and pancreatic cysts, cerebral and intracranial aneurysms, and cardiovascular abnormalities (Luciano and Dahl, 2014). Although mutations in PKD1, PKD2 (also called polycystin-1/2) or their dosage alterations account for ADPKD, their biophysical and physiological functions are not well understood (Douguet et al., 2019). PKD1 is a receptor-like membrane protein with 11 transmembrane (TM) segments (S1-S11) and a large extracellular N-terminus while PKD2 is a Ca^{2+}-permeable cation channel belonging to the transient receptor potential (TRP) superfamily of cation channels possessing six TMs (S1-S6) and pore domain S5-loop-S6 (Bergmann et al., 2018).PKD2 forms homotetramers but can also for heterotetramers to fulfill different functions (Cheng et al., 2010). As revealed by cryo-electron microscopy (EM) PKD1/PKD2 formed heterotetramers at 1:3 stoichiometry (Su et al., 2018). Through functional studies, we found that PKD1/PKD2 has higher Ca^{2+} permeability than homomeric PKD2 (Wang et al., 2019) but mechanisms of how PKD1 contributes to the selectivity filter and pore gate in PKD1/PKD2 remains elusive. It was reported that the extracellular N-terminus of PKD1 functions as an activation ligand of the PKD1/PKD2 complex (Ha et al., 2020). Additional reports demonstrated that PKD2 interacts with other ion channels including TRPV4 (Köttgen et al., 2008), TRPC1 (Kobori et al., 2009) and Piezo1 (Peyronnet et al., 2013) to form channel complexes with distinct biophysical properties. Nevertheless, how PKD2 is regulated by interacting partners remains largely unknown and deserves further studies.

TMEM120A (transmembrane protein 120A, also called TACAN) was initially reported as a nuclear envelope transmembrane protein critical for adipocyte differentiation (Batrakou et al., 2015). It was recently shown to form a mechano-sensitive ion channel sensing the pain (Beaulieu-Laroche et al., 2020), but this was challenged by subsequent structural and functional studies (Del Rosario et al., 2021; Ke et al., 2021; Niu et al., 2021; Parpaite et al., 2021; Rong et al., 2021; Xue et al., 2021). Global knockout of TACAN led to embryo death indicating its importance for embryonic development (Beaulieu-Laroche et al., 2020). Wide distribution of TACAN in non-neuronal tissues such as kidney, heart and intestine indicate its other plausible biological functions besides pain sensation (Beaulieu-Laroche et al., 2020). Previous proteomic screen suggested a potential interaction of PKD2 with TACAN (Sharif-Naeini et al., 2009) but their interaction and functional implications has yet to be explored and characterized

In the present study, we examined how TACAN modulates the PKD2 channel function using the two-electrode voltage clamp (TEVC) electrophysiology in *Xenopus* oocytes and single-channel patch clamp electrophysiology in Chinese hamster ovary (CHO) cells. We explored the subcellular localization of endogenous PKD2 and TACAN in different renal cell lines. We also characterized the interaction between TACAN and PKD2 by means of co-immunoprecipitation (co-IP) and immunofluorescence, and explored the relationship between physical association and functional regulation. Further, we examined how TACAN regulates PKD2 deficiency-associated disorders in zebrafish models by clustered regularly interspaced short palindromic repeats/CRISPR-associated protein 9 (CRISPR/Cas9).

72 # Results

73 ## Effects of TACAN on the PKD2 channel function

74 TACAN was indicated as a potential interactor of PKD2 through a proteomic screen using
75 smooth muscle cells (Sharif-Naeini et al., 2009). To determine whether and how TACAN
76 modulates the PKD2 channel function, we utilized *Xenopus* oocyte expression together with the
77 two-electrode voltage clamp (TEVC). The whole-cell channel activity of wild-type (WT) PKD2
78 in oocytes is hardly detectable in part due to its low expression on the plasma membrane and
79 unknown agonist, Therefore, we instead used the current mediated by PKD2 gain-of-function
80 (GOF) mutant F604P (Arif Pavel et al., 2016) as induced large currents in oocytes, we used
81 currents mediated by mutant F604P as a function readout, similarly as our previous studies
82 (Zheng et al., 2018a; Zheng et al., 2018b). We found that while oocytes expressing human
83 TACAN alone does not exhibit any significant increase in the current compared with water-
84 injected oocytes (Fig. 1A and B). Co-expression of human PKD2 mutant F604P with TACAN is
85 associated with significantly decreased current amplitudes compared with those with F604P
86 expressed alone (Fig. 1A and B). Our data from whole-cell immunofluorescence (Fig. 1C) and
87 biotinylation assays (Fig. 1D) indicated that TACAN did not significantly affect the surface
88 expression of F604P, suggesting TACAN inhibits the F604P function. Interestingly, expression
89 of F604P reduced both the total and surface expression of TACAN (Fig. 1E), but the underlying
90 mechanism remains unknown.

91 Next, we examined whether TACAN affected the F604P ion selectivity using extracellular
92 solutions containing 100 mM Na^+, Li^+, K^+ or non-permeable N-methyl-d-glucamine (NMDG,
93 negative control). We found that the reversal potential shifts due to solution changes for
94 F604P/TACAN but remain the same as those for F604P alone (Fig. 1F), indicating that TACAN
95 does not significantly affect the cation permeability ratios (with $P_{Na} : P_{Li} : P_K = 1 : 1.65 : 2.15$ for
96 F604P, consistent with previous reports (Shen et al., 2016) and $P_{Na} : P_{Li} : P_K = 1 : 1.66 : 2.15$ for
97 F604P/TACAN). Extracellular Ca^{2+} is known to reduce the PKD2 conductance to monovalent
98 cations (Arif Pavel et al., 2016; Shen et al., 2016). Here we found that Ca^{2+} exhibits a similar
99 inhibitory effect on F604P/TACAN and F604P alone (Fig. 1G and H). Taken together, our data
100 showed that TACAN inhibits the mutant F604P channel activity but does not affect the cation
101 selectivity or inhibition of F604P by extracellular Ca^{2+}.

102 To further characterize how TACAN inhibits the PKD2 channel function, we performed single-
103 channel patch clamp electrophysiology in CHO cells. Expression of TACAN with mutant F604P
104 or WT PKD2 substantially reduced the single-channel amplitude and open probability while
105 TACAN expressed alone did not induce any specific current under our experimental condition
106 (Fig. 2A and B), consistent with whole-cell data obtained using oocytes. We also noticed that at
107 +80 mV in the absence of TACAN the single-channel amplitude and open probability values for
108 PKD2 are significantly lower than those for mutant F604P, which may account for its much
109 lower whole-cell currents.

110 We next examined pressure sensitivity of PKD2 in CHO cells with or without co-expression of
111 TACAN. PKD2 in complex with PKD1 or TRPV4 was reported to be involved in mechano
112 sensing (Köttgen et al., 2008; Nauli et al., 2003) but whether PKD2, PKD1, TRPV4 or an
113 unknown binding protein senses mechanical stimuli is not well understood. With PKD2
114 expressed alone in CHO cells, pressure up to -30 mm Hg had no effect on the single-channel
115 amplitude or open probability (Fig. 2C). In contrast, in the presence of TACAN co-expression,

116 the open probability value significantly increased with negative pressure while the single-
117 channel current amplitude was insensitive to the pressure (Fig. 2D). These data showed that
118 channel complex PKD2/TACAN possesses mechano sensitivity mediated by TACAN, which the
119 single-channel open probability, but not the unitary current, stimulated by the pressure. Of note,
120 no channel activity was observed in cells expressing TACAN alone with pressure up to -30 mm
121 Hg (Fig. S1). Increasing the pressure beyond -30 mm Hg in our setup generated non-specific
122 leak currents, presumably due to broken cell membrane.

123 Besides inhibiting the F604P steady-state currents, TACAN induced significant inactivation of
124 the F604P-mediated currents at membrane depolarization (Fig. 3A). The steady-state current to
125 the peak current ratio for F604P alone was close to 1 (1.01 ± 0.01 at +100 mV, N = 7, p = 0.73),
126 i.e., there was no appreciable inactivation, while this ratio decreased to 0.67 ± 0.04 (N = 7, p <
127 0.001) with TACAN co-expression (Fig. 3B). The current inactivation at depolarizations (+50 to
128 +100 mV) in the presence of TACAN was voltage dependent, with time constant (τ) values in
129 the range of 139.23 ± 15.43 and 33.8 ± 4.80 ms (N = 7) obtained from exponential fits (Fig. 3C).
130 Interestingly, significant inactivation at polarized voltages was also present in PKD2 GOF gate
131 mutant L677G expressed alone (Fig. 3D). Unlike the F604P mutation, which locks PKD2 in an
132 activated configuration, the GOF of the L677G mutation is due to direct increases in the pore
133 hydrophilicity and size, which would infer that the L677G mutant protein may still be in a basal
134 configuration similar to WT PKD2 (Zheng et al., 2018b). Interestingly, although TACAN
135 significantly reduced the steady-state currents of L677G (Fig. 3D-F, it did not affect the
136 inactivating part of the L677G currents, which were associated with a similar range of
137 inactivation time constant compared with F604P/TACAN (Fig. 3G vs Fig. 3C). These data
138 together seemed to suggest that inactivation occurs when PKD2 protein is in an inhibited
139 (F604P+TACAN) or a basal state (L677G, with or without TACAN) but not in an activated state
140 (F604P alone).

141 **Physical interaction between PKD2 and TACAN**

142 TACAN was shown to be highly expressed in the kidney (Beaulieu-Laroche et al., 2020). We
143 checked the subcellular localization of PKD2 and TACAN by double immunofluorescence
144 assays in ciliated epithelia Madin-Darby Canine Kidney (MDCK), inner medullary collecting
145 duct (IMCD), and Lilly Laboratories Cell-Porcine Kidney 1 (LLC-PK1) cell lines. We found that
146 the endogenous PKD2 and TACAN both display enhanced staining in the primary cilia in all
147 three cell lines (Fig. 4A), indicating co-distribution of the two proteins. We also performed co-IP
148 experiments using these cell lines to assess their interaction and found that PKD2 is present in
149 the immunoprecipitates obtained with an anti-TMEM120A antibody, but not in those with IgG
150 (control) (Fig. 4B), demonstrating that PKD2 and TACAN are in the same protein complex in
151 these native cells.

152 We next characterized the physical interaction between PKD2 and TACAN interaction in
153 oocytes to better relate to our functional data. Indeed, TACAN co-immunoprecipitated TACAN
154 and mutant F604P in oocytes and reversely, mutant F604P was able to precipitate TACAN (Fig.
155 5A-C), indicating that PKD2 and TACAN are in the same complex in oocytes. We then used
156 chemical cross-linking to examine the subunit stoichiometry of the PKD2/TACAN complex.
157 However, the complex cannot be detected under our conditions although we successfully
158 detected TACAN dimers and different PKD2 oligomers (Fig. S2A). The coiled-coil domain
159 (amino-acid (aa) G9-L100) in the TACAN N-terminus was proposed to be important for
160 oligomerization (Batrakou et al., 2015). Indeed, we found aggregation of the N-terminus in our

161 chemical cross-linking experiments. Further, TACAN lacking the entire N-terminus still formed
162 the dimer (Fig. S2B), indicating that the TACAN dimeric assembly is independent of its coiled-
163 coil domain. Furthermore, we generated different fragments of TACAN, which possesses six
164 TMs (S1-S6), to narrow down the domain(s) mediating physical and functional interaction with
165 PKD2 (Fig. S3). By co-IP assays we found that TACAN fragments containing S1 (K135-T160)
166 or S6 (L296-D343), but not the N-terminus (K135X), interacts with PKD2 F604P (Fig. 5D).
167 While S1-containing TACAN fragments exhibited no functional effect on F604P, interestingly,
168 S6-containing fragments lacking the N-terminus exhibited significant inhibitory effects (Fig. 5E).
169 Further, this inhibition was even stronger than the one by full-length TACAN (Fig. 5E),
170 presumably because these fragments can't form dimers (Fig. S2B), which enhanced their
171 interaction with F604P.

172 Reversely, we tried to identify which part(s) in PKD2 is involved in the interaction with
173 TACAN. We performed co-IP experiments in CHO cells expressing TACAN together with the
174 PKD2 N-terminus (PKD2-N, M1-K215), C-terminus (PKD2-C, D682-V968), or PKD2 lacking
175 both the N- and C-termini (PKD2-TM, S209-K688). PKD2-TM but not PKD2-N or PKD2-C
176 conferred interaction with TACAN (Fig. 6A), which challenges the previous proteomic screen
177 study indicating that TACAN binds to the PKD2 C-terminus (Sharif-Naeini et al., 2009).

178 The PKD2 pore domain is formed by S5, S5-S6 loop and S6 (A594-Q693) (Shen et al., 2016).
179 We next examined whether TACAN participates in the pore formation in the PKD2/TACAN
180 channel complex. For this purpose, we tested whether TACAN interacts with truncation mutant
181 A594X (no pore domain) or fragment N580-L700 containing the pore domain (Fig. S3).
182 Surprisingly, TACAN can interact with either of them (Fig. 6B), indicating that PKD2 also
183 contains at least two domains interacting with TACAN. Because the TACAN S1 and S6
184 interacted with PKD2, we continued to narrow down the corresponding binding domains in
185 PKD2. We found by co-IP that PKD2 A594X interacts with TACAN S6, while PKD2 N580-
186 L700 interacts with TACAN S1 (Fig. 6C). Since the interaction between S6 was functionally
187 critical, it highly suggested that instead of acting as the pore formation subunit, TACAN mainly
188 binds at the peripheral domain (S1-S4) to regulate PKD2 channel function.

189 We wondered whether the PKD2/TACAN binding is required for inhibition of the PKD2
190 function by TACAN. For this, we co-expressed the TACAN N-terminus (K135X) in the
191 presence of F604P and TACAN, and indeed found that K135X represses the PKD2/TACAN
192 association (Fig. 7A), indicating that K135X acts as an effective blocking peptide, presumably
193 because it can compete with PKD2 for binding (dimerizing) with TACAN (see Fig. S2). Further,
194 K135K which had no functional effect on PKD2 (Fig. 5E) significantly represses the inhibition
195 of the PKD2 function by TACAN (Fig. 7B). Our data together thus demonstrated that inhibition
196 of the PKD2 function by TACAN is mediated by their physical association.

197 Regulation of the PKD2 function in zebrafish by TACAN

198 We next utilized zebrafish models to investigate the regulatory role *in vivo* of TACAN in PKD2.
199 Sufficient reduction in the PKD2 expression or function in larval zebrafish results in the presence
200 of tail curvature and pronephric cysts resembling renal cysts in mammals (Zheng et al., 2016).
201 Here, we employed the clustered regularly interspaced short palindromic repeats/CRISPR-
202 associated protein 9 (CRISPR/Cas9) technique and successfully knocked down the endogenous
203 PKD2 in larval fish at 3 days post-fertilization (dpf) through injection of 200 pg PKD2 sgRNA
204 and 300 pg Cas9 per embryo, which resulted in tail curling (Fig. 8A and B). We reasoned that if

205 we reduce the injected PKD2 sgRNA and Cas9 amounts there may be no or low occurrence of
206 tail curling but co-expression of TACAN may significantly aggravate the severity of the disease
207 if the PKD2 function is inhibited.

208 Indeed, while injection of 100 pg PKD2 sgRNA and 200 pg Cas9 per embryo was associated
209 with low percentage of fish with tail curling, co-expression of human TACAN through co-
210 injection on *in vitro* transcribed mRNA (100 pg/embryo) substantially increased the occurrence
211 of tail curling (Fig. 8C and D), consistent with the assumption that the PKD2 function is
212 inhibited by over-expressed TACAN, which was observed in oocytes and CHO cells. Our
213 Western blot experiments showed that the PKD2 expression is not significantly reduced by
214 TACAN over-expression (Fig. 8E), which is in agreement with our data from cellular models.
215 We also observed that TACAN over-expression alone did not significantly increase the
216 occurrence of tail curling (Fig. 8D), indicating that the functional inhibition of the endogenous
217 PKD2 by TACAN is in general insufficient to induce the disease. We also examined pronephric
218 cysts in larval fish and found that TACAN co-expression substantially increases the occurrence
219 of pronephric cysts while TACAN over-expression or PKD2 knockdown alone exhibits no or
220 low occurrence of pronephric cyst (Fig. 8F and G). Taken together, our data demonstrated that
221 TACAN aggravates PKD2-dependent disease severity in larval zebrafish, presumably through
222 repressing the PKD2 channel function.

Discussion

TACAN is a transmembrane protein that is evolutionally conserved and was recently reported to be involved in sensing mechanical stimuli (Beaulieu-Laroche et al., 2020). Its intracellular N-terminal coiled-coil domain (aa G9-L100) was reported to be important for oligomerization (Batrakou et al., 2015), consistent with our cross-linking results showing that deletion of the N-terminus significantly reduced its dimerization (Fig. S3A). However, the remaining dimers indicate the presence of another domain important for dimerization. While this other domain involved in homo-dimerization remains unknown, our current study showed that the TACAN TM domains S1 and S6 mediate binding with PKD2. Interestingly, while the PKD2 C-terminal coiled-coil domain was reported to be involved in interaction with PKD1 (Qian et al., 1997; Tsiokas et al., 1997; Yu et al., 2009), heterotetrameric PKD1/PKD2 structure was revealed by cryo-EM in the absence of the PKD2 coiled-coil domain (Su et al., 2018), demonstrating that the domain is not essential for the PKD1/PKD2 complexing. In fact, we here showed that the PKD2 TMs but not its N- or C-terminus interacts with the TACAN S1 and S6.

Besides homotetramerization, PKD2 can heteromerize with PKD1 and TRP channels including TRPC1, -C3, -C4, -C7 and -V4 (Cheng et al., 2010; Grieben et al., 2017; Shen et al., 2016). PKD2 homo-and heterotetrameric channels have distinct biophysical properties as well as distinct subcellular localizations (Cheng et al., 2010). The PKD1/PKD2 heterotetrameric channel defective in ADPKD has a 1:3 stoichiometry (Su et al., 2018). While it is well known that PKD1 promotes the plasma membrane trafficking of PKD2, how it contributes to the channel pore formation is not well understood (Ha et al., 2020; Wang et al., 2019). PKD1/PKD2 located in renal epithelial primary cilia was previously shown to mediate mechano-dependent Ca^{2+} entry(Nauli et al., 2003) but subsequent studies found that, controversially, the Ca^{2+} entry is PKD1-independent (Liu et al., 2018). PKD2/TRPC4 in the MDCK primary cilia was found to be involved in flow sensing but the role of primary cilia and mammalian TRP channels in mechano sensing remains debatable (Delling et al., 2016; Köttgen et al., 2008; Nikolaev et al., 2019). Our current study found that in the PKD2/TACAN channel complex TACAN but not PKD2 confers mechano sensitivity (Fig. 2D). It will be interesting to investigate whether TACAN plays a role in the pathogenesis of ADPKD.

Mammalian TACAN (TMEM120A) and its homologue TMEM120B (70.5% sequence identity) are generated as a result of gene duplication. However, when they were expressed in CHO cells, only TACAN induced mechano-sensitive currents (Beaulieu-Laroche et al., 2020). TACAN, but not TMEM120B, was reported to inhibit the Piezo2 channel function (Del Rosario et al., 2021). It will be of interest to determine whether TMEM120B regulates the PKD2 function in future studies.

Zebrafish has a relatively simple renal system called pronephros that develop within 24 hours post-fertilization (hpf) and represents an established PKD model with easy visualization of organs and tissues with transparent embryos and larvae, and the ability for rapid phenotype analysis. PKD2 knockdown (KD) by injection of morpholino antisense oligonucleotides (MO) in zebrafish embryos results in tail curling and pronephric cysts at 3-5 days post-fertilization (dpf) (Zheng et al., 2016). However, because MO knockdown may have off-target effects, in the present study we knocked down PKD2 by CRISPR/Cas9, which is known to be more specific than MO knockdown. Our study using larval zebrafish demonstrated that TACAN aggravates the severity of PKD2 insufficiency-dependent diseases, presumably through repressing the PKD2

267 function but not the expression, consistent with its regulatory effect on PKD2 using cellular
268 models.

269 Interestingly, it was reported that TMEM33, an activator of PKD2, which forms a complex on
270 the endoplasmic reticulum (ER) membrane, but not in primary cilia, fails to regulate PKD2-
271 dependent pronephric renal cystogenesis in zebrafish (Arhatte et al., 2019), indicating that PKD2
272 located on the ER membrane is not involved in cystogenesis. Thus, the colocalization or
273 interaction of PKD2 and TACAN in the renal primary cilia may be important for TACAN to
274 confer its regulatory role in PKD2 and the associated disease phenotypes in zebrafish.

275 The report that TACAN acts as an ion channel has been challenged by recent structural and
276 functional studies (Beaulieu-Laroche et al., 2020; Del Rosario et al., 2021; Ke et al., 2021; Niu et
277 al., 2021; Parpaite et al., 2021; Rong et al., 2021; Xue et al., 2021). However, the concept that
278 TACAN is an ion channel is supported by a recent report showing that a point mutation at a
279 candidate pore gate residue significantly increases the channel activity (Chen et al., 2021) and
280 that, by molecular dynamic simulations, each TACAN monomer contains an ion conducting
281 pathway but multiple subunits might be required for TACAN to form a functional ion channel.
282 Also, TACAN was shown to be involved in regulation of ion transport based on its involvement
283 in regulation of the expression of different proteins including Ca^{2+} ATPase, ATP2a1 and
284 TMEM150C, a general regulator of mechano-sensitive channels such as Piezo1, Piezo2 and the
285 potassium channel TREK-1 (Anderson et al., 2018). Structural studies found that TACAN
286 structure resembles that of the long-chain fatty acid elongase 7 (Ke et al., 2021; Niu et al., 2021;
287 Rong et al., 2021; Xue et al., 2021), suggesting the possibility that TACAN may act as an
288 enzyme. In addition to our current finding, TACAN was previously reported to be an inhibitor of
289 Piezo2, but not Piezo1 or TREK-1, but with an unclear mechanism of inhibition (Del Rosario et
290 al., 2021).

291 In summary, our present study found that TACAN inhibits the PKD2 function through the
292 physical PKD2/TACAN association. It is unlikely that TACAN participates in the pore
293 formation in the PKD2/TACAN channel complex since TACAN-S6 that doesn't seem to be
294 sufficient for contributing to pore formation still exhibited an inhibitory effect. As a novel
295 regulator of PKD2, TACAN inhibits PKD2 *in vitro* and *in vivo*. Blocking peptides such as
296 K135X may eventually lead to specific peptide molecules with therapeutic potential for ADPKD.

297 # Methods

298 **Plasmids, reagents and antibodies**

299 HA-tagged human PKD2 (HA-PKD2) in vector pGEMHE for *Xenopus* oocyte expression and
300 PKD2 mutant F604P in vector pcDNA3.1 for mammalian cell expression were obtained from
301 Dr. Yong Yu (St. John's University, NY). Human HA-TACAN in a modified pCMV vector for
302 mammalian cell expression, a kind gift from Dr. Reza Sharif-Naeini (McGill University, QC,
303 Canada), was subcloned into vector PGEMHE for oocyte expression, with a 5' Flag tag. Human
304 PKD2, PKD2-N, PKD2-TM and PKD2-C in vector pEGFP for oocyte expression were
305 constructed previously (Wang et al., 2012). All mutations were carried out using Q5 High-
306 Fidelity 2X Master Mix from New England Biolabs (NEB, Ottawa, ON, Canada) and verified by
307 sequencing. Antibodies against β-actin and Arl13b were from Santa Cruz Biotechnology (Santa
308 Cruz, CA) and those against Flag, HA, TMEM120A and PKD2 were from Proteintech Group
309 (Rosemont, IL). Secondary antibodies were purchased from GE Healthcare (Waukesha, WI).
310 DTT was purchased from Thermo Fisher Scientific (Ottawa, ON, Canada) and disuccinimidyl
311 tartrate (DST) from CovaChem (Loves Park, IL).

312 ***Xenopus* oocyte expression**

313 Capped RNAs encoding human PKD2, human TACAN or their mutants were synthesized by *in*
314 *vitro* transcription using the T7 mMESSAGE mMACHINE kit (Invitrogen, Waltham, MA) and
315 injected into oocytes (25 ng each), as described (Cai et al., 2020). Control oocytes were injected
316 with the same amount of water. Oocytes were incubated at 18℃ for 2-3 days before
317 measurements. The present study was approved by the Ethical Committee for Animal
318 Experiments of the University of Alberta and performed in accordance with the Guidelines for
319 Research with Experimental Animals of the University of Alberta and the Guide for the Care and
320 Use of Laboratory Animals (NIH Guide) revised in 1996.
321

322 **Culture and transfection of mammalian cells**

323 CHO cells were cultured in Dulbecco's Modified Eagle Medium/Nutrient Mixture F-12
324 (DMEM/F12) supplemented with L-glutamine, penicillin-streptomycin and 10% fetal bovine
325 serum (FBS). MDCK, IMCD and LLC-PK1 cells were cultured in DMEM supplemented with L-
326 glutamine, penicillin-streptomycin and 10% FBS. All cultured cells were kept at 37°C with 5%
327 CO_2. Transfection of cDNAs was performed using Lipofectamine 3000 (Invitrogen) according to
328 the manufacturer's protocol.

329 **Two-electrode voltage clamp**

330 The two-electrode voltage clamp electrophysiology experiments in *Xenopus* oocytes were
331 performed as we described previously (Zheng et al., 2018a) Briefly, an electrode made of a
332 capillary glass pipette (Warner Instruments, Hamden, CT) was filled with 3 M KCl and impaled
333 an oocyte to form a tip resistance of 0.3-2 MΩ. The Geneclamp 500B amplifier and Digidata
334 1322A AD/DA converter (Molecular Devices, Union City, CA) were used to record the whole-
335 cell currents and membrane potentials. The pClamp 9 software (Axon Instruments, Union City,
336 CA) was used to acquire and analyze the data. Both signals were digitized at 200 μs/sample and
337 filtered at 2 kHz through a Bessel filter. Data were plotted using SigmaPlot 13 (Systat Software,
338 San Jose, CA) or GraphPad Prism 8 (GraphPad Software, San Diego, CA).

339 **Patch clamp**

340 Patch-clamp recordings were carried out as we described previously (Fatehi et al., 2017), under
341 voltage clamp at room temperature (~22°C). The recording pipette and chamber were coupled by
342 Ag/AgCl electrodes to an Axopatch 200B patch-clamp amplifier and Digidata 1200A BNC data-
343 acquisition system, controlled by pCLAMP 10 software (Axon Instruments). Both bath and
344 pipette solutions were composed of (in mM) 140 NaCl, 5 KCl, 2 $CaCl_2$, 2 $MgCl_2$, 10 HEPES, 10
345 glucose and pH 7.4. The seal resistance was no less than 5 GΩ for all cell-attached recordings.
346 The recordings were low-pass filtered at 1 kHz following acquisition. Linear stepwise negative
347 pressures (by suction) of various magnitudes were applied to the interior of the glass pipette
348 using a high-speed pressure clamp system (HSPC-1, ALA Scientific, Farmingdale, NY).

349 **Western blot and surface protein biotinylation**

350 *Xenopus* oocytes after 3-times washing with ice-cold PBS solution were incubated with 0.5
351 mg/ml sulfo-NHS-SS-Biotin (Pierce, Rockford, IL) for 30 min at room temperature. Non-reacted
352 biotin was quenched by 1 M NH_4Cl. Oocytes were then washed with ice-cold PBS solution and
353 harvested in ice-cold CelLytic M lysis buffer (Sigma-Aldrich, St. Louis, MO) supplemented with
354 proteinase inhibitor cocktail (Thermo Fisher Scientific). Upon addition of 100 µl streptavidin
355 (Pierce) lysates were incubated at 4℃ overnight with gentle shaking. The surface protein bound
356 to streptavidin was resuspended in SDS loading buffer and subjected to SDS-PAGE.

357 **Chemical cross-linking**

358 Chemical cross-linking assays were performed as previously described (Yu et al., 2009). Oocytes
359 expressing desired proteins were harvested in ice-cold CelLytic M lysis buffer (Sigma-Aldrich)
360 supplemented with proteinase inhibitor cocktail (Thermo Fisher Scientific). Fresh crosslinker
361 stock solutions were prepared by dissolving DST (CovaChem) into dimethylsulfoxide (Sigma-
362 Aldrich). Cross-linking reactions were carried out by diluting the stock solution into the cell
363 lysate samples, followed by incubation on ice for 4 h. SDS loading buffer was used to stop the
364 reactions. The samples were incubated at 37 °C for 30 min and subjected to SDS-PAGE.

365 **Immunofluorescence**

366 Whole-mount immunofluorescence assays using *Xenopus* oocytes were performed as described
367 (Zheng et al., 2018a). Briefly, oocytes were washed in PBS, fixed in 4% paraformaldehyde for
368 15 min, washed three times in PBS plus 50 mM NH_4Cl, and then permeabilized with 0.1%
369 Triton X-100 for 4 min. Oocytes were then blocked in PBS plus 3% skim milk for 30 min and
370 then incubated overnight with indicated primary antibodies, followed by incubation with
371 secondary Alexa-488-conjugated donkey anti-rabbit or Cy3-conjugated goat anti-mouse antibody
372 (Jackson ImmunoResearch Laboratories, West Grove, PA) for 30 min. Oocytes were then
373 mounted in Vectashield (Vector Labs, Burlington, ON, Canada) and examined on an AIVI
374 spinning disc confocal microscopy (Cell Imaging Facility, Faculty of Medicine and Dentistry,
375 University of Alberta).

376 **Co- IP**

377 Co-IP experiments were performed as we previously described (Zheng et al., 2018a). Briefly, a
378 group of 20-30 oocytes washed with PBS were solubilized in ice-cold CelLytic-M lysis buffer
379 (Sigma-Aldrich) supplemented with proteinase inhibitor cocktail. Supernatants were collected
380 after centrifugation at 13,200 rpm for 15 min and precleaned for 1 h with 50% protein G-
381 Sepharose (GE Healthcare), followed by incubation with an indicated antibody at 4℃ for 4 h.
382 Upon addition of 100 µl of 50% protein G-Sepharose, the mixture was incubated at 4℃

383 overnight with gentle shaking. The immune complexes conjugated to protein G-Sepharose were
384 washed three times with cold PBS solution containing 1% Nonidet P-40 and eluted by SDS
385 loading buffer. Precipitated proteins were subjected to Western blot analysis.

386 **Zebrafish experiments**

387 Zebrafish experiments were modified from one described previously (Zheng et al., 2018b).
388 Briefly, embryos of WT zebrafish AB line were grown at 28.5 ºC in water supplemented with 60
389 μg/ml Instant Ocean Sea salts. Single guide RNAs (sgRNAs: AGAACACCGCTCTAGTGCCG)
390 targeting the first coding exon of zebrafish PKD2 was designed and synthesized. The Cas9
391 protein was purchased from NEB. Mixture of sgRNA (100 pg) and Cas9 (200 pg) was injected
392 into each fertilized embryo at 1-2 hpf for PKD2 knock down. The effect of injected
393 CRISPR/Cas9 was confirmed by sequencing. Human TACAN mRNA was injected into
394 fertilized embryos at 1-2 hpf at 100 pg each. This study has been approved by the Hubei
395 University of Technology animal welfare regulations and maintained according to standard
396 protocols (http://ZFIN.org).
397 Histological analysis was performed as previously reported (Wang et al., 2020). Briefly, embryos
398 at 3 dpf were anesthetized in tricaine solution and fixed in 4% PFA at 4 ºC. After 3-times wash
399 (20 min each) in cold PBS, embryos were decalcified in EDTA solution (684 mM EDTA, pH
400 8.0) and then washed (2 × 20 min) with DEPC solution and dehydrated through graded alcohol.
401 Before paraffin processing, embryos were embedded in 1% agarose (Sigma-Aldrich) in TAE
402 buffer (Thermo Fisher Scientific). Subsequently, samples were sectioned transversely at 5 μm
403 thickness using a HM325 manual rotary microtome (Thermo Fisher Scientific). H&E staining
404 was processed with Varistain TM Gemini ES Automated Slide Stainer (Thermo Fisher
405 Scientific).

406 **Statistical analysis**

407 All statistical data in this study were represented as mean ± SEM (standard error of the mean)
408 from N measurements. Student's t-test was used for two groups comparisons and one-way
409 ANOVA for multiple groups comparisons. *, ** and *** indicate $p < 0.05$, 0.01 and 0.001,
410 respectively; ns indicates statistically not significant.

411 **Author contributions**
412 Conceptualization, X.L., and X.-Z.C.; Investigation, X.L., R.Z., M.F., Y.W., W.L., R.T., X.D.,
413 Z.W., Q.X.; Supervision, P.R.L., J.T., and X.-Z.C. Writing, X.L., and X.-Z.C.

414 **Acknowledgments**
415 We would like to thank Dr. Reza Sharif-Naeini for sharing TACAN related plasmids. This work
416 was supported by the Natural Sciences and Engineering Research Council of Canada (NSERC),
417 the Kidney Foundation of Canada (to X.Z.C.) and National Natural Science Foundation of China
418 (grant #32070726, to J.T.). X.L. was a recipient of the Alberta Graduate Excellence Scholarship.

419 **Declaration of Interests**
420 The authors declare no competing interests.

421 **Figure legends**

422 **Figure 1. Functional regulation of PKD2 by TACAN in *Xenopus* oocytes**. **A.** Representative
423 current traces obtained using a voltage jump protocol in oocytes expressing TACAN, PKD2
424 F604P (F604P for short) or F604P + TACAN, in the presence of the divalent-free Na-containing
425 solution (in mM): 100 NaCl, 2 KCl, 10 HEPES and pH 7.5. Data from water-injected oocytes
426 served as negative control (Ctrl). **B.** Statistical bar graphs of currents recoded at +80 mV
427 obtained under the same experimental conditions as in **A**. Data are presented as mean ± SEM. * p
428 < 0.05; ** p < 0.01. **C.** Representative IF images showing oocyte surface expression of TACAN
429 or F604P. Scale bar, 50 mm. **D.** Representative Western blot data of the biotinylated (surface)
430 and total protein of F604P and TACAN. **E.** Averaged data obtained as those from **D** (n = 3).
431 Data are presented as mean ± SEM. ns, not significant; *** p < 0.001. **F.** Upper panel:
432 representative I-V curves for F604P or F604P + TACAN when 100 mM of an indicated ion was
433 used in the divalent ion-free bath solution. Lower panel: averaged reversal potentials. Data are
434 presented as mean ± SEM. ns, not significant. **G** and **H.** Left panel: representative I-V curves for
435 PKD2 F604P (**G**) and F604P + TACAN (**H**) in bath solution with or without 1 mM Ca^{2+}. Right
436 panel: effect of Ca^{2+} on the inward (-80 mV) and outward (+80 mV) currents for F604P (**G**) and
437 F604P + TACAN (**H**). Data are presented as mean ± SEM. * p < 0.05; ** p < 0.01; *** p <
438 0.001.

439 **Figure 2. Effects of TACAN and pressure on PKD2 single-channel parameters in CHO**
440 **cells. A.** Representative single-channel recordings (at +80 mV) of CHO cells with indicated
441 transfections. The same solution (in mM: 140 NaCl, 5 KCl, 2 $CaCl_2$, 2 $MgCl_2$, 10 HEPES, 10
442 glucose, and pH 7.4) was used in the pipette and bath. **B.** Quantified unitary current amplitudes
443 and open probabilities obtained from **A**. Data are presented as mean ± SEM. ** p < 0.01; *** p <
444 0.001. **C** and **D.** Left panels: representative single-channel recordings (at +80 mV) in CHO cells
445 transfected with PKD2 (**C**) or PKD2 + TACAN (**D**) showing the effect of negative pressures.
446 Right panels: effect of the pressure on the unitary currents and normalized open probabilities of
447 PKD2 (**C**) or PKD2 + TACAN (**D**). Data are presented as mean ± SEM. ns, not significant; ** p
448 < 0.01.

449 **Figure 3. Effect of TACAN on inactivation of PKD2-mediated currents in oocytes. A.**
450 Representative traces from oocytes expressing PKD2 F604P or F604P + TACAN. Traces
451 obtained from +50 mV to +100 mV were marked blue or green, as indicated. For clarity, those at
452 +80 mV were compared. **B.** Ratios of the steady currents (I_{steady}) to the peak currents (I_{peak}) for
453 F604P and F604P + TACAN obtained as in **A**. **C.** Time constant (τ) of current decay for F604P
454 + TACAN obtained through an exponential fit (N = 7). **D.** Representative traces from oocytes
455 expressing PKD2 L677G or L677G + TACAN. Traces obtained from +50 mV to +100 mV are
456 marked blue or green, as indicated. **E.** Left panel: Representative I-V curves from oocytes
457 expressing L677G or L677G + TACAN. Right panel: averaged currents at +80 mV obtained
458 from oocytes expressing L677G or L677G + TACAN. Data are presented as mean ± SEM. ** p<
459 0.01. **F.** Representative Western blot data of the surface (biotinylated) and total proteins of
460 L677G and TACAN. **G.** Time constants (τ) of current decay for L677G and L677G + TACAN
461 (N = 5).

462 **Figure 4. Colocalization and association of the endogenous PKD2 and TACAN in renal cell**
463 **lines. A.** Subcellular localization of the endogenous PKD2 and TACAN in MDCK, IMCD and
464 LLC-PK1 cells by means of immunofluorescence. Arl13b served as a primary cilia marker. Scale

465 bar, 5 μm. **B.** Representative co-IP data showing association between the endogenous PKD2 and
466 TACAN in MDCK, IMCD and LLC-PK1 cells.

467 **Figure 5. Domains of TACAN mediating association with PKD2. A and B.** Representative
468 co-IP data showing the interaction between PKD2 mutant HA-F604P and Flag-TACAN using
469 Flag antibody (**A**) or PKD2 antibody (**B**) for precipitation. **C.** Representative co-IP data showing
470 interaction between WT HA-PKD2 and Flag-TACAN using Flag antibody for precipitation. **D.**
471 Representative co-IP data showing the interaction between mutant HA-F604P and an indicated
472 TACAN truncation mutant using Flag antibody for precipitation. **E.** Representative I-V curves
473 and averaged currents at +80 mV in oocytes expressing F604P with or without a TACAN
474 truncation mutant. Data are presented as mean ± SEM. * $p < 0.05$; ** $p < 0.01$; *** $p < 0.001$.

475 **Figure 6. Domains in PKD2 mediating association with TACAN. A.** Left panels:
476 representative co-IP data showing the interaction between GFP-PKD2 and HA-TACAN using
477 HA antibody for precipitation. Non-transfected and GFP-transfected CHO cell lysates served as
478 negative controls. Right panel: binding strength averaged from three independent experiments.
479 **B.** Representative co-IP data showing the interaction between Flag-TACAN and a PKD2
480 truncation mutant (A594X or N580-L700) using Flag antibody for precipitation. PKD2
481 expressed in oocytes with or without co-expressed Flag-TACAN served as positive and negative
482 controls, respectively. **C.** Representative co-IP data showing the interaction between PKD2
483 mutant A594X and TACAN mutant L296-D343, and between PKD2 mutant N580-L700 and
484 TACAN mutant K160X using Flag antibody for precipitation. PKD2 mutants A594X and N580-
485 L700 alone served as negative controls.

486 **Figure 7. Effect of the TACAN N-terminus on TACAN's inhibition of the PKD2 function.**
487 **A.** Left panel: representative I-V curves from oocytes expressing F604P, F604P + TACAN, or
488 F604P + TACAN + TACAN N-terminus (K135X). Right panel: averaged currents at +80 mV.
489 Data are presented as mean ± SEM. ns, not significant, *** $p < 0.001$. **B.** Representative co-IP
490 data showing the effect of K135X on the association between PKD2 and TACAN.

491 **Figure 8. Effect of TACAN on the tail curling and pronephric cystogenesis of larval**
492 **zebrafish. A.** Left panel: schematic presentation of the PKD2 protein/gene domain architecture
493 and CRISPR target sites. The gene loci are shown with exons (gray boxes) and introns (solid
494 lines). The position of the CRISPR target sites in exon 1 in the PKD2 gene and the
495 corresponding PKD2 protein (black box) are indicated by the dash lines, and the predicted
496 remaining (truncated) PKD2 protein (PKD2 CRISPR) is indicated. Right panel: sequencing of
497 PKD2 in the Ctrl and PKD2 CRISPR fish at 3 dpf. Red lines indicate CRISPR target sites. **B.**
498 Upper panel: PKD2 protein detected by Western blot under the Ctrl (water injection) and
499 CRISPR-directed PKD2 knock down (KD) conditions (PKD2 sgRNA 200 pg + Cas9 300 pg) at
500 3 dpf. Lower panels: representative pictures of embryos at 3 dpf. **C.** Representative pictures
501 showing tails of 3 dpf zebrafish under the Ctrl, TACAN overexpression (OE) (by injection of
502 mRNA at100 pg each), or PKD2 KD condition. **D.** Average percentages of fish displaying curled
503 tail under different conditions. Data were from three independent experiments with the indicated
504 total numbers of embryos. ns, not significant, ***$p < 0.001$. **E.** Representative Western blot data
505 showing the expression of PKD2 and TACAN. **F.** Representative pictures of a 3-dpf embryo with
506 PKD2 KD plus TACAN OE, showing pronephric cyst formation (red box and arrow). Ctrl fish
507 was injected with water only. Cyst formation was also indicated by a histologic section showing

508 dilated pronephric tubules (asterisks). G, glomerulus; Pt, pronephric tubule. **G.** Averaged
509 percentages of embryos exhibiting pronephric cysts under the indicated conditions. Data are
510 presented as mean ± SEM. ***$p < 0.001$.
511

512 **References**
513
514 Anderson, E.O., Schneider, E.R., Matson, J.D., Gracheva, E.O., and Bagriantsev, S.N. (2018).
515 TMEM150C/Tentonin3 Is a Regulator of Mechano-gated Ion Channels. Cell reports *23*, 701-
516 708. 10.1016/j.celrep.2018.03.094.
517 Arhatte, M., Gunaratne, G.S., El Boustany, C., Kuo, I.Y., Moro, C., Duprat, F., Plaisant, M.,
518 Duval, H., Li, D., Picard, N., et al. (2019). TMEM33 regulates intracellular calcium homeostasis
519 in renal tubular epithelial cells. Nature communications *10*, 2024. 10.1038/s41467-019-10045-y.
520 Arif Pavel, M., Lv, C., Ng, C., Yang, L., Kashyap, P., Lam, C., Valentino, V., Fung, H.Y.,
521 Campbell, T., Møller, S.G., et al. (2016). Function and regulation of TRPP2 ion channel revealed
522 by a gain-of-function mutant. Proceedings of the National Academy of Sciences of the United
523 States of America *113*, E2363-2372. 10.1073/pnas.1517066113.
524 Batrakou, D.G., de Las Heras, J.I., Czapiewski, R., Mouras, R., and Schirmer, E.C. (2015).
525 TMEM120A and B: Nuclear Envelope Transmembrane Proteins Important for Adipocyte
526 Differentiation. PloS one *10*, e0127712. 10.1371/journal.pone.0127712.
527 Beaulieu-Laroche, L., Christin, M., Donoghue, A., Agosti, F., Yousefpour, N., Petitjean, H.,
528 Davidova, A., Stanton, C., Khan, U., Dietz, C., et al. (2020). TACAN Is an Ion Channel Involved
529 in Sensing Mechanical Pain. Cell *180*, 956-967.e917. 10.1016/j.cell.2020.01.033.
530 Bergmann, C., Guay-Woodford, L.M., Harris, P.C., Horie, S., Peters, D.J.M., and Torres, V.E.
531 (2018). Polycystic kidney disease. Nature reviews. Disease primers *4*, 50. 10.1038/s41572-018-
532 0047-y.
533 Cai, R., Liu, X., Zhang, R., Hofmann, L., Zheng, W., Amin, M.R., Wang, L., Hu, Q., Peng, J.B.,
534 Michalak, M., et al. (2020). Autoinhibition of TRPV6 Channel and Regulation by PIP2. iScience
535 *23*, 101444. 10.1016/j.isci.2020.101444.
536 Chen, X., Wang, Y., Li, Y., Lu, X., Chen, J., Li, M., Wen, T., Liu, N., Chang, S., Zhang, X., et
537 al. (2021). Cryo-EM structure of the human TACAN channel in a closed state. bioRxiv,
538 2021.2008.2023.457436. 10.1101/2021.08.23.457436.
539 Cheng, W., Sun, C., and Zheng, J. (2010). Heteromerization of TRP channel subunits: extending
540 functional diversity. Protein & cell *1*, 802-810. 10.1007/s13238-010-0108-9.
541 Del Rosario, J.S., Gabrielle, M., Yudin, Y., and Rohacs, T. (2021). TMEM120A/TACAN
542 inhibits mechanically activated Piezo2 channels. bioRxiv, 2021.2006.2030.450616.
543 10.1101/2021.06.30.450616.
544 Delling, M., Indzhykulian, A.A., Liu, X., Li, Y., Xie, T., Corey, D.P., and Clapham, D.E. (2016).
545 Primary cilia are not calcium-responsive mechanosensors. Nature *531*, 656-660.
546 10.1038/nature17426.
547 Douguet, D., Patel, A., and Honoré, E. (2019). Structure and function of polycystins: insights
548 into polycystic kidney disease. Nature reviews. Nephrology *15*, 412-422. 10.1038/s41581-019-
549 0143-6.
550 Fatehi, M., Carter, C.C., Youssef, N., and Light, P.E. (2017). The mechano-sensitivity of cardiac
551 ATP-sensitive potassium channels is mediated by intrinsic MgATPase activity. Journal of
552 molecular and cellular cardiology *108*, 34-41. 10.1016/j.yjmcc.2017.05.004.
553 Grieben, M., Pike, A.C., Shintre, C.A., Venturi, E., El-Ajouz, S., Tessitore, A., Shrestha, L.,
554 Mukhopadhyay, S., Mahajan, P., Chalk, R., et al. (2017). Structure of the polycystic kidney
555 disease TRP channel Polycystin-2 (PC2). Nature structural & molecular biology *24*, 114-122.
556 10.1038/nsmb.3343.

557 Ha, K., Nobuhara, M., Wang, Q., Walker, R.V., Qian, F., Schartner, C., Cao, E., and Delling, M.
558 (2020). The heteromeric PC-1/PC-2 polycystin complex is activated by the PC-1 N-terminus.
559 eLife *9*. 10.7554/eLife.60684.
560 Harris, P.C., and Torres, V.E. (2009). Polycystic kidney disease. Annual review of medicine *60*,
561 321-337. 10.1146/annurev.med.60.101707.125712.
562 Ke, M., Yu, Y., Zhao, C., Lai, S., Su, Q., Yuan, W., Yang, L., Deng, D., Wu, K., Zeng, W., et al.
563 (2021). Cryo-EM structures of human TMEM120A and TMEM120B. Cell discovery *7*, 77.
564 10.1038/s41421-021-00319-5.
565 Kobori, T., Smith, G.D., Sandford, R., and Edwardson, J.M. (2009). The transient receptor
566 potential channels TRPP2 and TRPC1 form a heterotetramer with a 2:2 stoichiometry and an
567 alternating subunit arrangement. The Journal of biological chemistry *284*, 35507-35513.
568 10.1074/jbc.M109.060228.
569 Köttgen, M., Buchholz, B., Garcia-Gonzalez, M.A., Kotsis, F., Fu, X., Doerken, M., Boehlke, C.,
570 Steffl, D., Tauber, R., Wegierski, T., et al. (2008). TRPP2 and TRPV4 form a polymodal sensory
571 channel complex. The Journal of cell biology *182*, 437-447. 10.1083/jcb.200805124.
572 Liu, X., Vien, T., Duan, J., Sheu, S.H., DeCaen, P.G., and Clapham, D.E. (2018). Polycystin-2 is
573 an essential ion channel subunit in the primary cilium of the renal collecting duct epithelium.
574 eLife *7*. 10.7554/eLife.33183.
575 Luciano, R.L., and Dahl, N.K. (2014). Extra-renal manifestations of autosomal dominant
576 polycystic kidney disease (ADPKD): considerations for routine screening and management.
577 Nephrology, dialysis, transplantation : official publication of the European Dialysis and
578 Transplant Association - European Renal Association *29*, 247-254. 10.1093/ndt/gft437.
579 Nauli, S.M., Alenghat, F.J., Luo, Y., Williams, E., Vassilev, P., Li, X., Elia, A.E., Lu, W.,
580 Brown, E.M., Quinn, S.J., et al. (2003). Polycystins 1 and 2 mediate mechanosensation in the
581 primary cilium of kidney cells. Nature genetics *33*, 129-137. 10.1038/ng1076.
582 Nikolaev, Y.A., Cox, C.D., Ridone, P., Rohde, P.R., Cordero-Morales, J.F., Vasquez, V., Laver,
583 D.R., and Martinac, B. (2019). Mammalian TRP ion channels are insensitive to membrane
584 stretch. Journal of cell science *132*. 10.1242/jcs.238360.
585 Niu, Y., Tao, X., Vaisey, G., Olinares, P.D.B., Alwaseem, H., Chait, B.T., and MacKinnon, R.
586 (2021). Analysis of the mechanosensor channel functionality of TACAN. eLife *10*.
587 10.7554/eLife.71188.
588 Parpaite, T., Brosse, L., Séjourné, N., Laur, A., Mechioukhi, Y., Delmas, P., and Coste, B.
589 (2021). Patch-seq of mouse DRG neurons reveals candidate genes for specific mechanosensory
590 functions. Cell reports *37*, 109914. 10.1016/j.celrep.2021.109914.
591 Peyronnet, R., Martins, J.R., Duprat, F., Demolombe, S., Arhatte, M., Jodar, M., Tauc, M.,
592 Duranton, C., Paulais, M., Teulon, J., et al. (2013). Piezo1-dependent stretch-activated channels
593 are inhibited by Polycystin-2 in renal tubular epithelial cells. EMBO reports *14*, 1143-1148.
594 10.1038/embor.2013.170.
595 Qian, F., Germino, F.J., Cai, Y., Zhang, X., Somlo, S., and Germino, G.G. (1997). PKD1
596 interacts with PKD2 through a probable coiled-coil domain. Nature genetics *16*, 179-183.
597 10.1038/ng0697-179.
598 Rong, Y., Jiang, J., Gao, Y., Guo, J., Song, D., Liu, W., Zhang, M., Zhao, Y., Xiao, B., and Liu,
599 Z. (2021). TMEM120A contains a specific coenzyme A-binding site and might not mediate
600 poking- or stretch-induced channel activities in cells. eLife *10*. 10.7554/eLife.71474.

601 Sharif-Naeini, R., Folgering, J.H., Bichet, D., Duprat, F., Lauritzen, I., Arhatte, M., Jodar, M.,
602 Dedman, A., Chatelain, F.C., Schulte, U., et al. (2009). Polycystin-1 and -2 dosage regulates
603 pressure sensing. Cell *139*, 587-596. 10.1016/j.cell.2009.08.045.
604 Shen, P.S., Yang, X., DeCaen, P.G., Liu, X., Bulkley, D., Clapham, D.E., and Cao, E. (2016).
605 The Structure of the Polycystic Kidney Disease Channel PKD2 in Lipid Nanodiscs. Cell *167*,
606 763-773.e711. 10.1016/j.cell.2016.09.048.
607 Su, Q., Hu, F., Ge, X., Lei, J., Yu, S., Wang, T., Zhou, Q., Mei, C., and Shi, Y. (2018). Structure
608 of the human PKD1-PKD2 complex. Science (New York, N.Y.) *361*. 10.1126/science.aat9819.
609 Tsiokas, L., Kim, E., Arnould, T., Sukhatme, V.P., and Walz, G. (1997). Homo- and
610 heterodimeric interactions between the gene products of PKD1 and PKD2. Proceedings of the
611 National Academy of Sciences of the United States of America *94*, 6965-6970.
612 10.1073/pnas.94.13.6965.
613 Wang, Q., Dai, X.Q., Li, Q., Wang, Z., Cantero Mdel, R., Li, S., Shen, J., Tu, J.C., Cantiello, H.,
614 and Chen, X.Z. (2012). Structural interaction and functional regulation of polycystin-2 by
615 filamin. PloS one *7*, e40448. 10.1371/journal.pone.0040448.
616 Wang, X., Giusti, A., Ny, A., and de Witte, P.A. (2020). Nephrotoxic Effects in Zebrafish after
617 Prolonged Exposure to Aristolochic Acid. Toxins *12*. 10.3390/toxins12040217.
618 Wang, Z., Ng, C., Liu, X., Wang, Y., Li, B., Kashyap, P., Chaudhry, H.A., Castro, A., Kalontar,
619 E.M., Ilyayev, L., et al. (2019). The ion channel function of polycystin-1 in the polycystin-
620 1/polycystin-2 complex. EMBO reports *20*, e48336. 10.15252/embr.201948336.
621 Xue, J., Han, Y., Baniasadi, H., Zeng, W., Pei, J., Grishin, N.V., Wang, J., Tu, B.P., and Jiang,
622 Y. (2021). TMEM120A is a coenzyme A-binding membrane protein with structural similarities
623 to ELOVL fatty acid elongase. eLife *10*. 10.7554/eLife.71220.
624 Yu, Y., Ulbrich, M.H., Li, M.H., Buraei, Z., Chen, X.Z., Ong, A.C., Tong, L., Isacoff, E.Y., and
625 Yang, J. (2009). Structural and molecular basis of the assembly of the TRPP2/PKD1 complex.
626 Proceedings of the National Academy of Sciences of the United States of America *106*, 11558-
627 11563. 10.1073/pnas.0903684106.
628 Zheng, W., Cai, R., Hofmann, L., Nesin, V., Hu, Q., Long, W., Fatehi, M., Liu, X., Hussein, S.,
629 Kong, T., et al. (2018a). Direct Binding between Pre-S1 and TRP-like Domains in TRPP
630 Channels Mediates Gating and Functional Regulation by PIP2. Cell reports *22*, 1560-1573.
631 10.1016/j.celrep.2018.01.042.
632 Zheng, W., Shen, F., Hu, R., Roy, B., Yang, J., Wang, Q., Zhang, F., King, J.C., Sergi, C., Liu,
633 S.M., et al. (2016). Far Upstream Element-Binding Protein 1 Binds the 3' Untranslated Region of
634 PKD2 and Suppresses Its Translation. Journal of the American Society of Nephrology : JASN
635 *27*, 2645-2657. 10.1681/ASN.2015070836.
636 Zheng, W., Yang, X., Hu, R., Cai, R., Hofmann, L., Wang, Z., Hu, Q., Liu, X., Bulkley, D., Yu,
637 Y., et al. (2018b). Hydrophobic pore gates regulate ion permeation in polycystic kidney disease 2
638 and 2L1 channels. Nature communications *9*, 2302. 10.1038/s41467-018-04586-x.

639

Fig 1

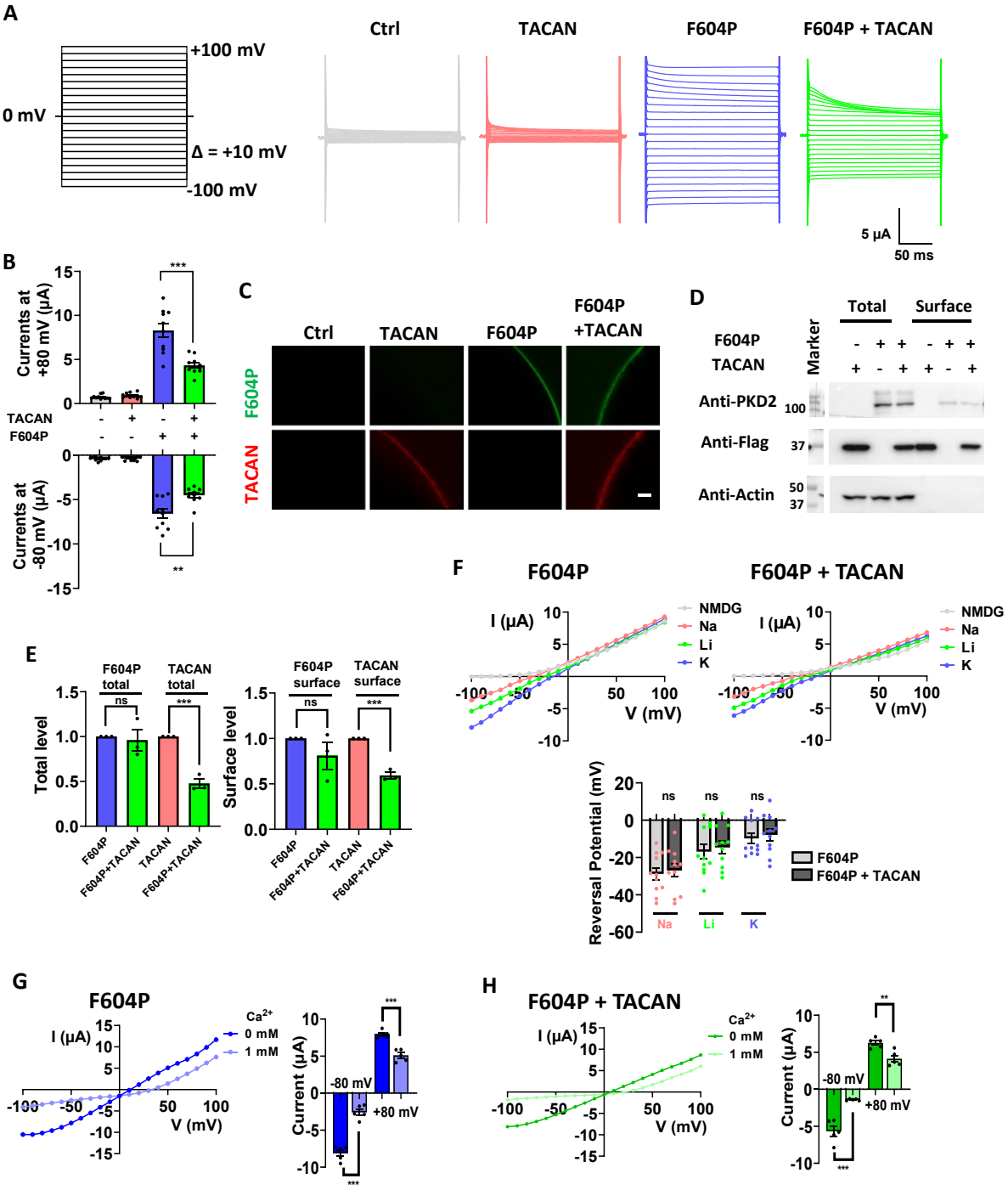
A
+100 mV
0 mV
Δ = +10 mV
-100 mV
Ctrl
TACAN
F604P
F604P + TACAN
5 µA
50 ms
B
Currents at +80 mV (µA)
Currents at -80 mV (µA)
TACAN
F604P
C
Ctrl
TACAN
F604P
F604P +TACAN
F604P
TACAN
D
Total
Surface
Marker
F604P
TACAN
Anti-PKD2
Anti-Flag
Anti-Actin
E
F604P total
TACAN total
F604P surface
TACAN surface
Total level
Surface level
F
F604P
F604P + TACAN
I (µA)
V (mV)
NMDG
Na
Li
K
Reversal Potential (mV)
F604P
F604P + TACAN
G
F604P
Ca2+
0 mM
1 mM
Current (µA)
-80 mV
+80 mV
H
F604P + TACAN

Fig 2

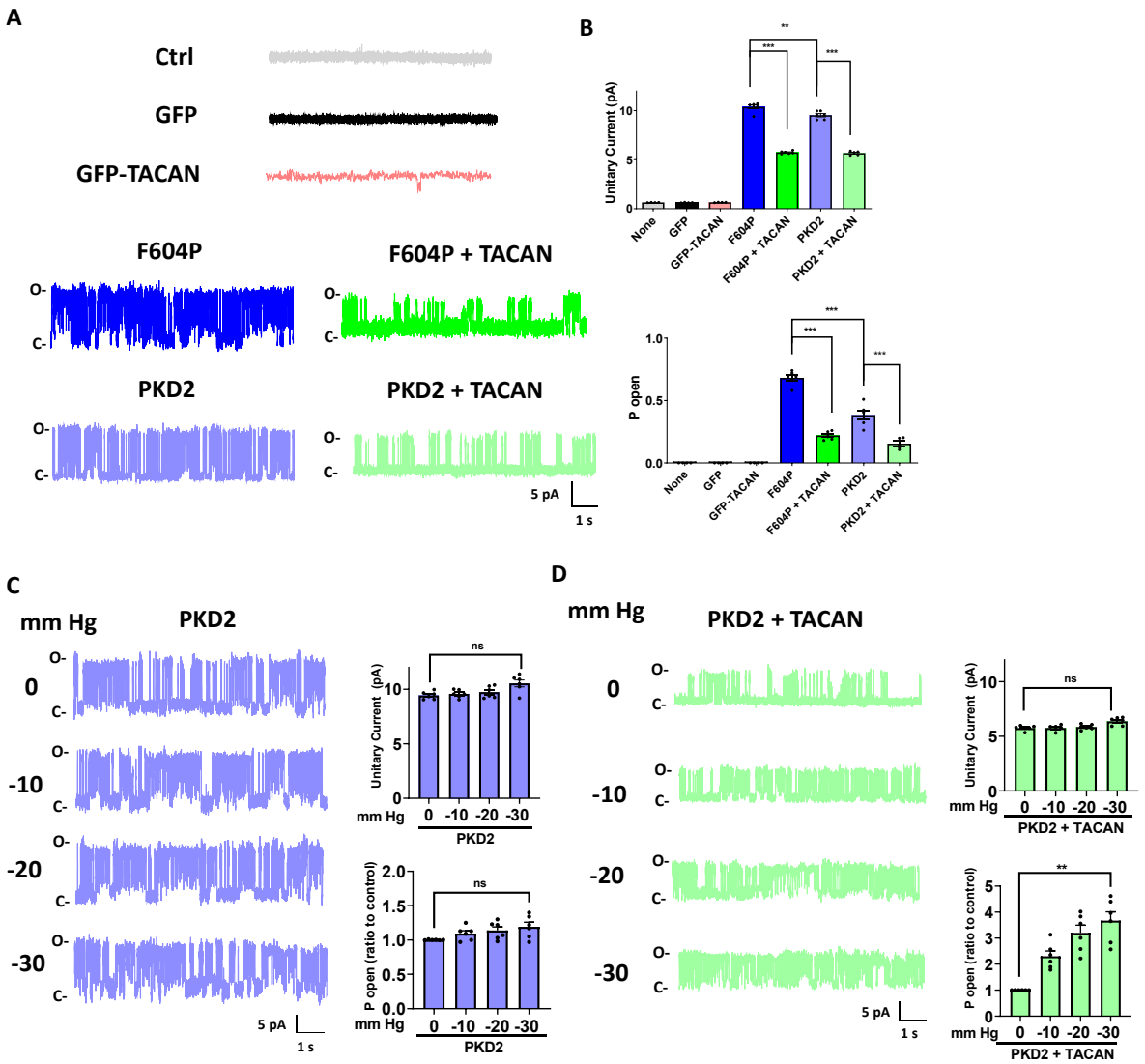
A
Ctrl
GFP
GFP-TACAN
F604P
F604P + TACAN
PKD2
PKD2 + TACAN
O-
C-
5 pA
1 s
B
Unitary Current (pA)
P open
None
GFP
GFP-TACAN
F604P
F604P + TACAN
PKD2
PKD2 + TACAN
C
mm Hg
PKD2
0
-10
-20
-30
ns
Unitary Current (pA)
P open (ratio to control)
D
PKD2 + TACAN
**

642

643

Fig 3

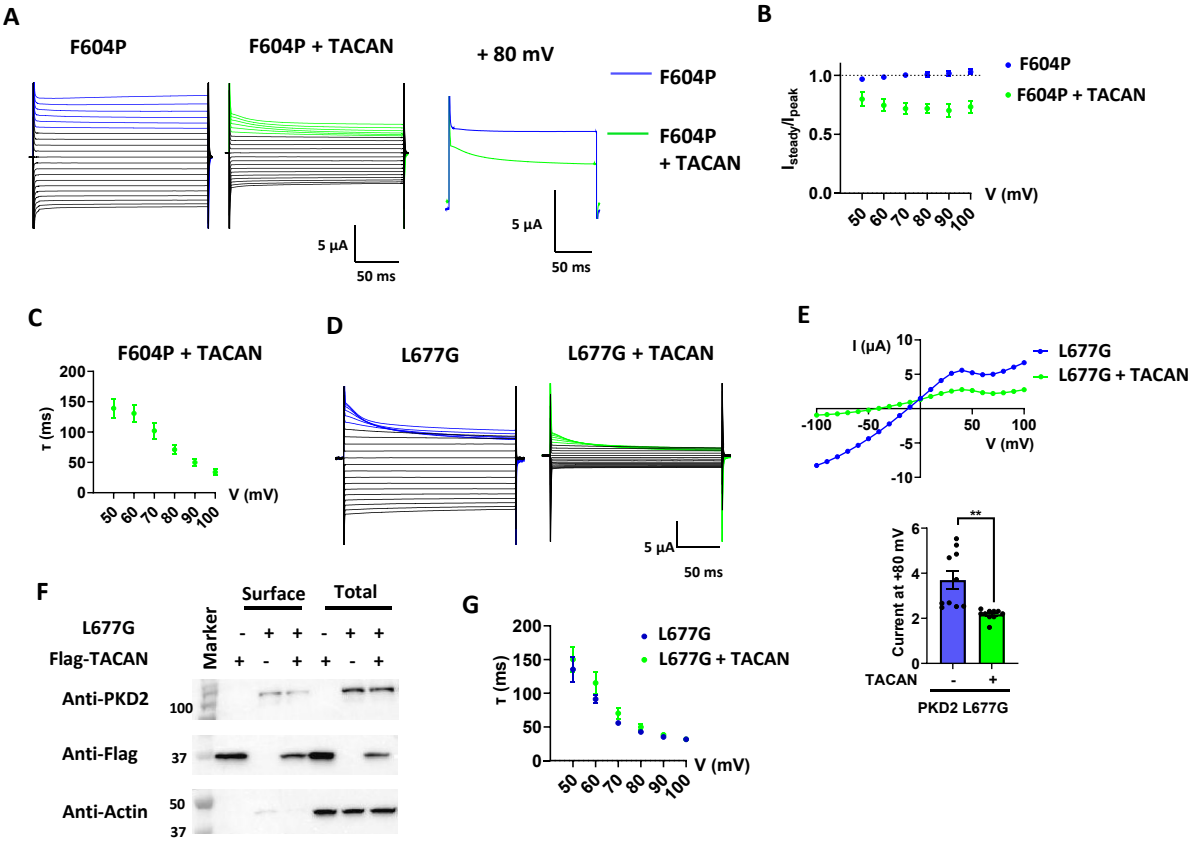
A
F604P
F604P + TACAN
+ 80 mV
F604P
F604P + TACAN
5 µA
50 ms
5 µA
50 ms
B
F604P
F604P + TACAN
1.0
0.5
0.0
V (mV)
50 60 70 80 90 100
C
F604P + TACAN
τ (ms)
200
150
100
50
0
V (mV)
50 60 70 80 90 100
D
L677G
L677G + TACAN
5 µA
50 ms
E
I (µA)
10
5
-5
-10
-100 -50 50 100
V (mV)
L677G
L677G + TACAN
Current at +80 mV
6
4
2
0
**
TACAN
-
+
PKD2 L677G
F
Surface
Total
L677G
Flag-TACAN
Marker
Anti-PKD2
100
Anti-Flag
37
Anti-Actin
50
37
G
τ (ms)
200
150
100
50
0
V (mV)
50 60 70 80 90 100
L677G
L677G + TACAN

644

645

Fig 4

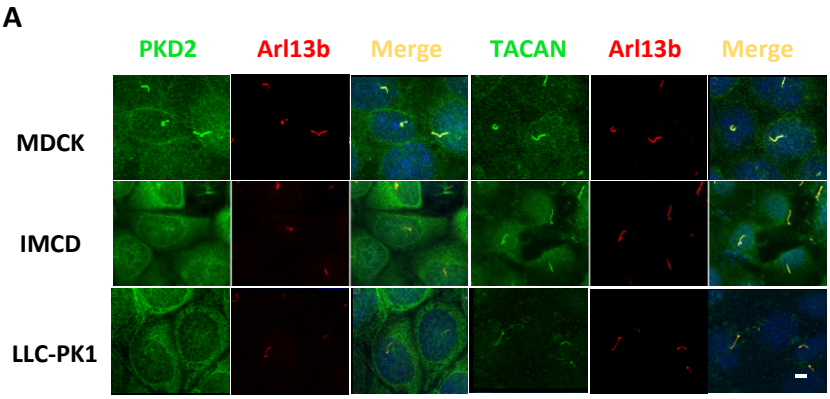
A
PKD2
Arl13b
Merge
TACAN
Arl13b
Merge
MDCK
IMCD
LLC-PK1

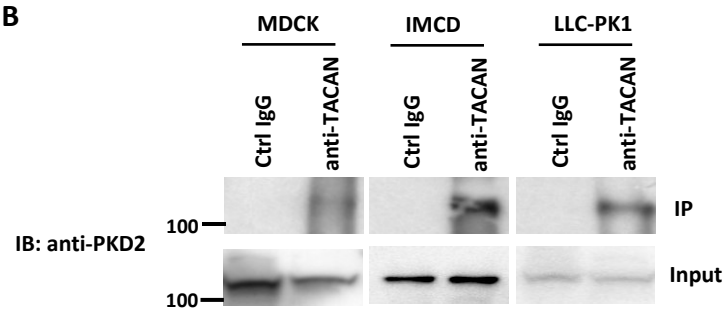
B
MDCK
IMCD
LLC-PK1
Ctrl IgG
anti-TACAN
Ctrl IgG
anti-TACAN
Ctrl IgG
anti-TACAN
IB: anti-PKD2
100
100
IP
Input

646

647

Fig 5

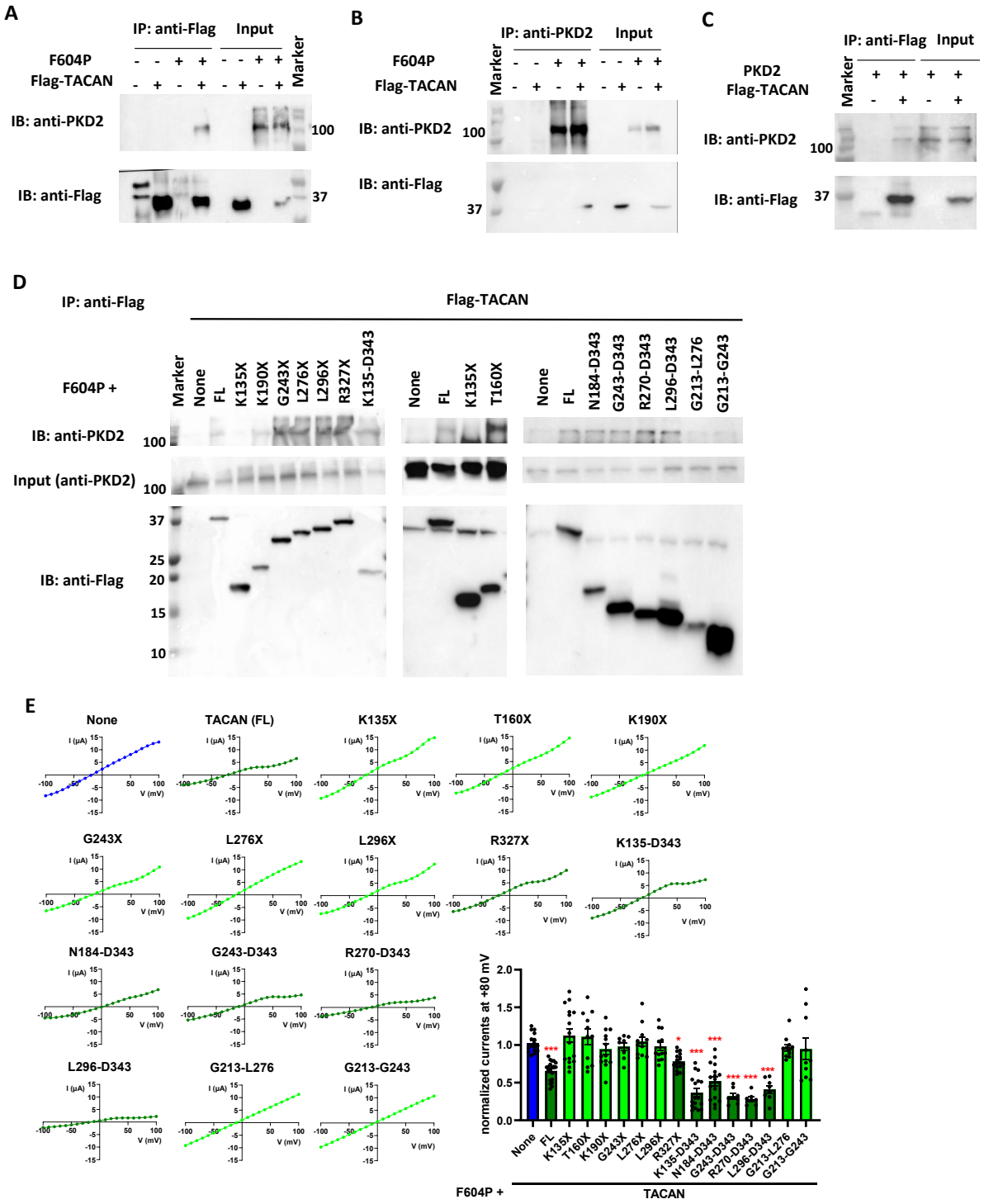
A
IP: anti-Flag
Input
F604P
Flag-TACAN
Marker
IB: anti-PKD2
IB: anti-Flag
100
37
B
IP: anti-PKD2
Input
F604P
Flag-TACAN
Marker
IB: anti-PKD2
IB: anti-Flag
100
37
C
IP: anti-Flag
Input
PKD2
Flag-TACAN
Marker
IB: anti-PKD2
IB: anti-Flag
100
37
D
IP: anti-Flag
Flag-TACAN
F604P +
Marker
None
FL
K135X
K190X
G243X
L276X
L296X
R327X
K135-D343
None
FL
K135X
T160X
None
FL
N184-D343
G243-D343
R270-D343
L296-D343
G213-L276
G213-G243
IB: anti-PKD2
Input (anti-PKD2)
IB: anti-Flag
100
100
37
25
20
15
10
E
None
TACAN (FL)
K135X
T160X
K190X
G243X
L276X
L296X
R327X
K135-D343
N184-D343
G243-D343
R270-D343
L296-D343
G213-L276
G213-G243
I (μA)
V (mV)
normalized currents at +80 mV
2.0
1.5
1.0
0.5
0.0
None
FL
K135X
T160X
K190X
G243X
L276X
L296X
R327X
K135-D343
N184-D343
G243-D343
R270-D343
L296-D343
G213-L276
G213-G243
F604P +
TACAN

Fig 6

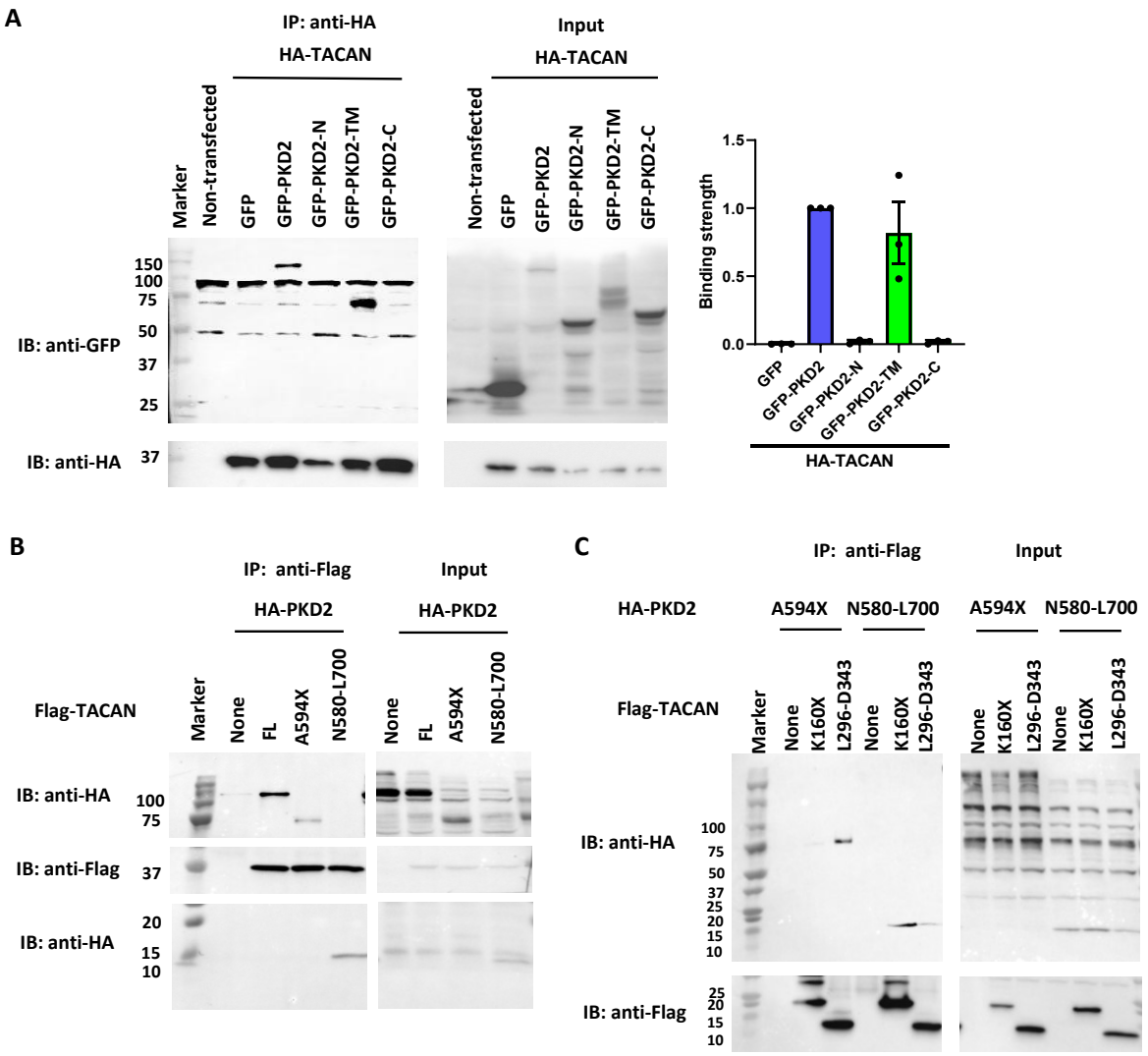
A
IP: anti-HA
HA-TACAN
Input
HA-TACAN
Marker
Non-transfected
GFP
GFP-PKD2
GFP-PKD2-N
GFP-PKD2-TM
GFP-PKD2-C
IB: anti-GFP
IB: anti-HA
150
100
75
50
37
25
Binding strength
1.5
1.0
0.5
0.0
B
IP: anti-Flag
Input
HA-PKD2
Flag-TACAN
None
FL
A594X
N580-L700
IB: anti-HA
IB: anti-Flag
20
15
10
C
A594X
N580-L700
K160X
L296-D343

650

651

Fig 7

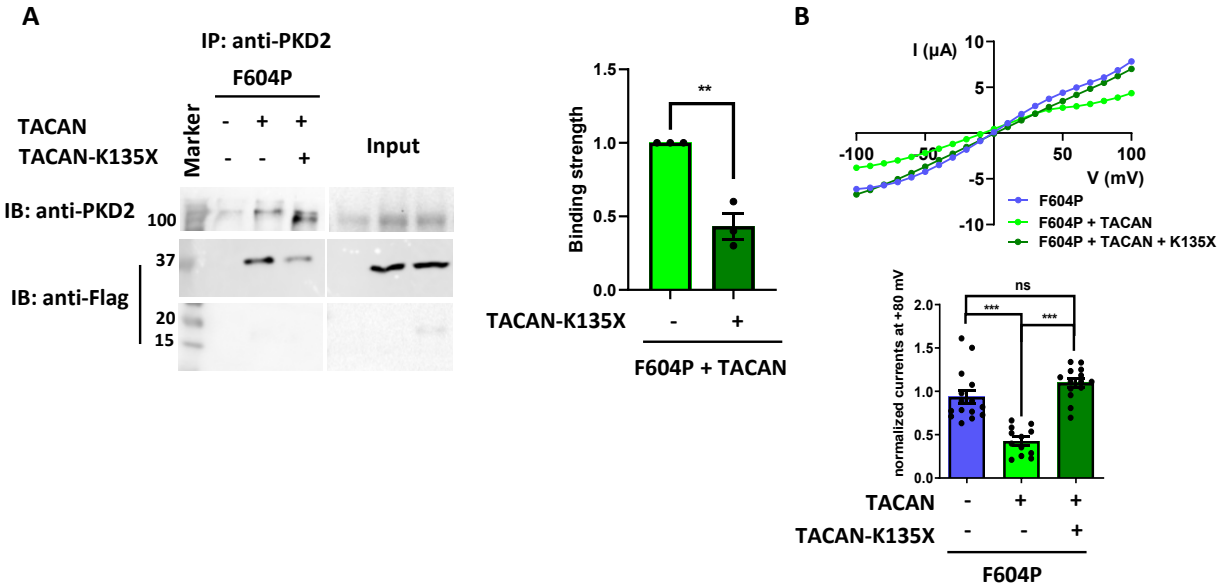
A
IP: anti-PKD2
F604P
TACAN
TACAN-K135X
Marker
Input
IB: anti-PKD2
100
37
IB: anti-Flag
20
15
Binding strength
TACAN-K135X
F604P + TACAN
B
I (μA)
V (mV)
F604P
F604P + TACAN
F604P + TACAN + K135X
normalized currents at +80 mV
ns
TACAN
TACAN-K135X
F604P

652

653

Fig 8

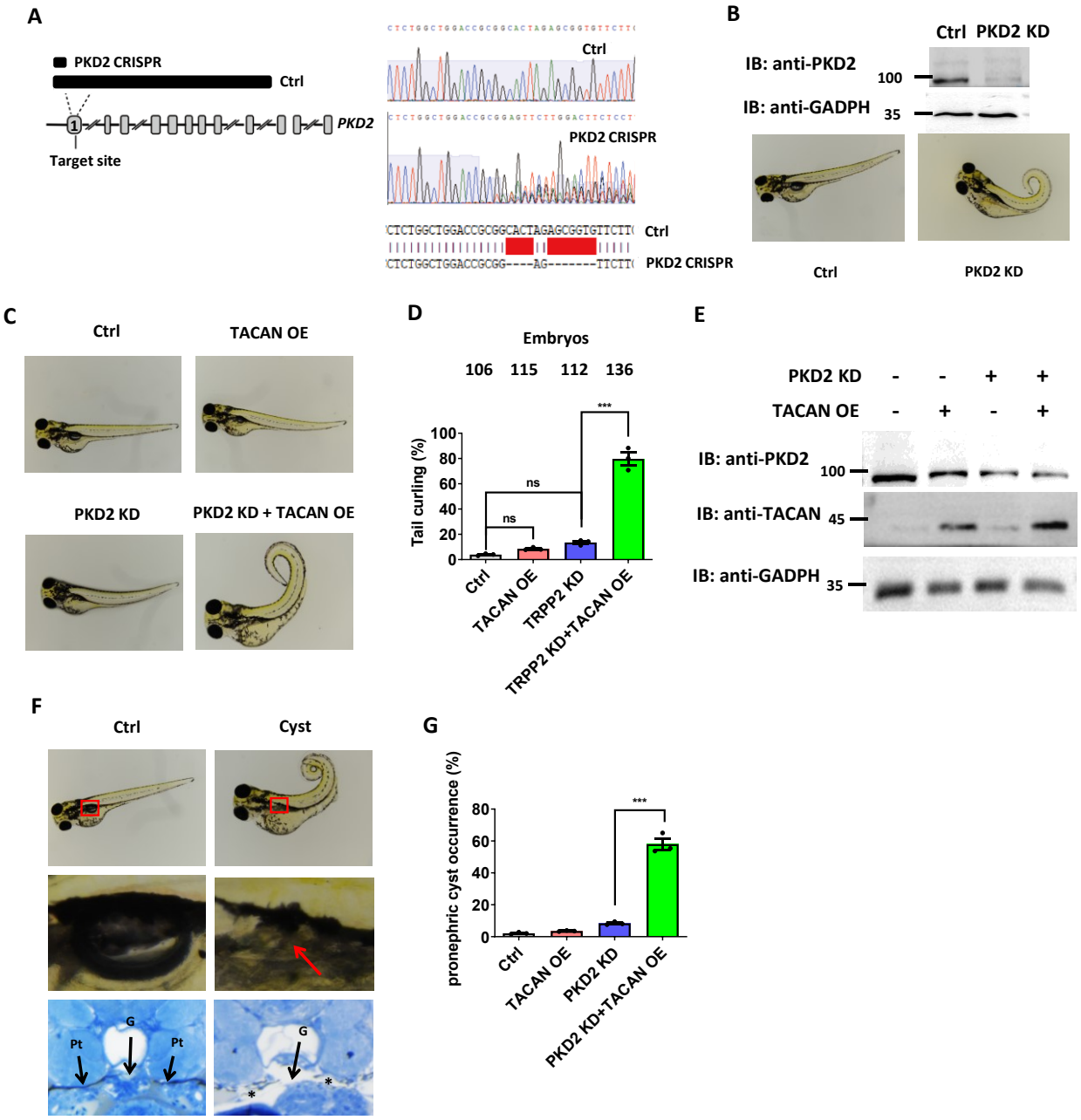
A
PKD2 CRISPR
Ctrl
PKD2
Target site
Ctrl
PKD2 CRISPR
CTCTGGCTGGACCGCGGCACTAGAGCGGTGTTCTT
CTCTGGCTGGACCGCGG----AG-------TTCTT
B
Ctrl PKD2 KD
IB: anti-PKD2
IB: anti-GADPH
100
35
Ctrl
PKD2 KD
C
Ctrl
TACAN OE
PKD2 KD
PKD2 KD + TACAN OE
D
Embryos
106 115 112 136
Tail curling (%)
ns
ns
***
Ctrl
TACAN OE
TRPP2 KD
TRPP2 KD+TACAN OE
E
PKD2 KD - - + +
TACAN OE - + - +
IB: anti-PKD2
IB: anti-TACAN
IB: anti-GADPH
100
45
35
F
Ctrl
Cyst
Pt
G
Pt
G
*
*
G
pronephric cyst occurrence (%)
***
Ctrl
TACAN OE
PKD2 KD
PKD2 KD+TACAN OE

654

655

Fig S1

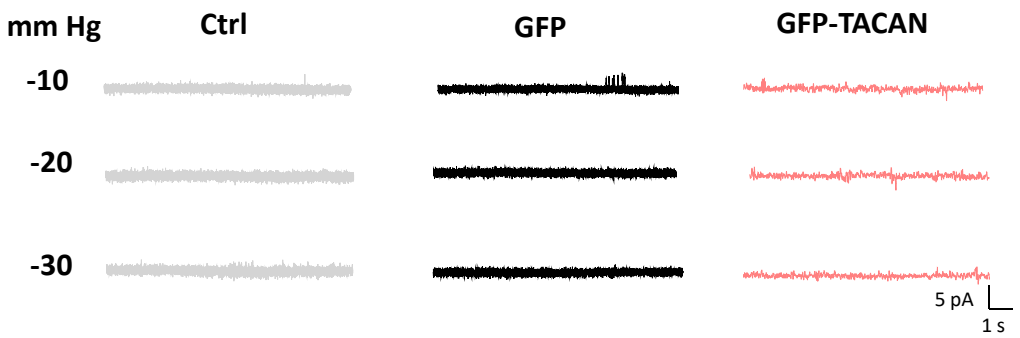

Figure S1. Channel activity of TACAN in CHO cells under negative pressures, related to Figure 2. Representative single channel recordings in CHO cells transfected with none (Ctrl), GFP or GFP-TACAN, in the presence of a negative pressure, as indicated.

Fig S2

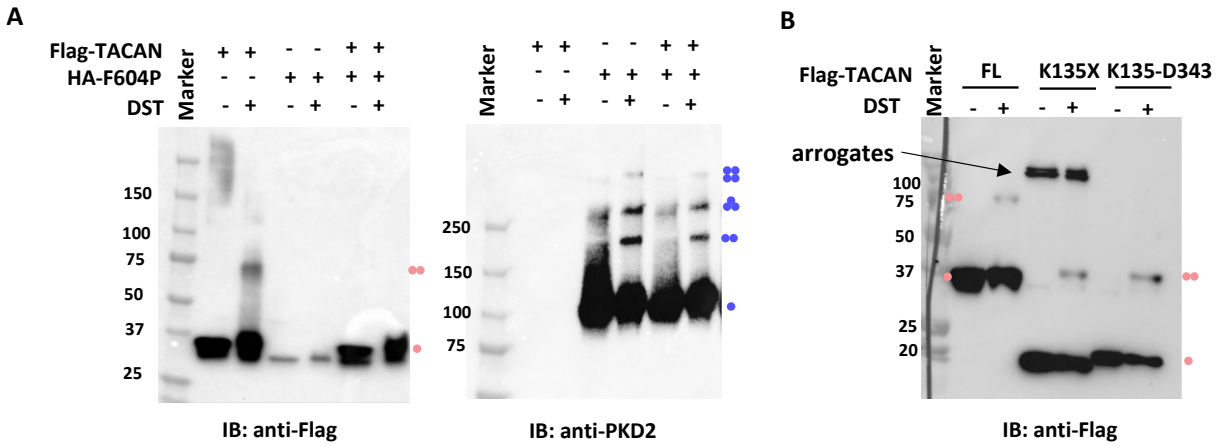

Figure S2. Oligomerization of TACAN and PKD2 F604P, related to Figure 4. A. Western blot data obtained in the presence of cross-linking, showing expression of TACAN and PKD2 F604P. Cross-linking was carried out with 1 mM disuccinimidyl tartrate (DST). Putative subunit composition of the bands is indicated. **B.** Western blot data obtained in the presence of cross-linking, showing expression of TACAN FL, K135X, and K135X-D343. Putative oligomer conditions are indicated.

Fig S3

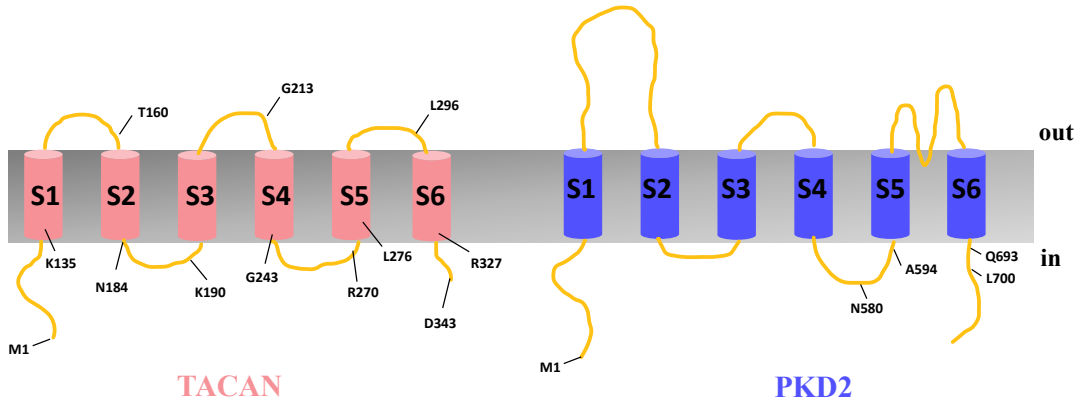

Figure S3. Topology of human TACAN and PKD2, related to Figure 4 and 5. Residues and their sites indicate the positions of the key truncation mutants used in the study.